

Control of Amphiphile Self-Assembly via Bioinspired Metal Ion Coordination

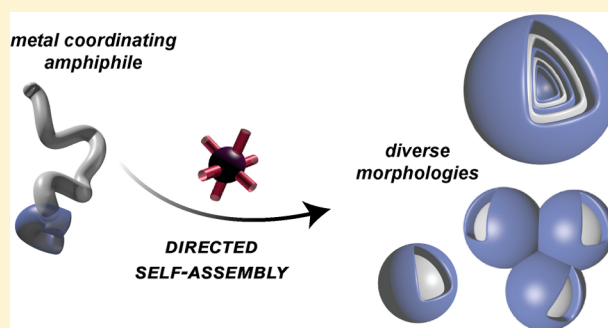
Abigail S. Knight,^{*,†} Josefin Larsson,[†] Jing M. Ren,[†] Raghida Bou Zerdan,[†] Shay Seguin,[†] Remy Vrahas,[†] Jianfang Liu,[§] Gang Ren,[§] and Craig J. Hawker^{*,†,‡,§}

[†]California NanoSystems Institute and Materials Research Laboratory and [‡]Materials Department and Department of Chemistry and Biochemistry, University of California, Santa Barbara, California 93106, United States

[§]The Molecular Foundry, Lawrence Berkeley National Laboratory, Berkeley, California 94720, United States

Supporting Information

ABSTRACT: Inspired by marine siderophores that exhibit a morphological shift upon metal coordination, hybrid peptide–polymer conjugates that assemble into different morphologies based on the nature of the metal ion coordination have been designed. Coupling of a peptide chelator, hexahistidine, with hydrophobic oligostyrene allows a modular strategy to be established for the efficient synthesis and purification of these tunable amphiphiles (oSt(His)₆). Remarkably, in the presence of different divalent transition metal ions (Mn, Co, Ni, Cu, Zn, and Cd) a variety of morphologies were observed. Zinc(II), cobalt(II), and copper(II) led to aggregated micelles. Nickel(II) and cadmium(II) produced micelles, and multilamellar vesicles were obtained in the presence of manganese(II). This work highlights the significant potential for transition metal ion coordination as a tool for directing the assembly of synthetic nanomaterials.



INTRODUCTION

Living organisms exploit a variety of stimuli to create nanoscale, responsive materials leading to complex macroscale functions. Structural change in response to a stimulus is critical for such functions (e.g., the release of a signaling molecule in a cascade or active transport across a membrane). Significantly, these dynamic responses allow for an array of structures/functions to be derived from a limited set of building blocks. In the pursuit of synthetic nanomaterials with comparable functionality, a toolbox of strategies including materials that respond to light,¹ pH,² temperature,³ and chemical⁴ stimuli has been developed. These strategies provide a valuable foundation for the development of responsive materials, but thus far they are largely limited to generating structures that interchange between two morphologies in response to various stimuli.

Transition metal ions are a unique tool for engineering responsive character based on their various binding stoichiometries and geometries, allowing a single material to have a diverse set of responses to different metal ions. This allows structural control in small molecules^{5–8} and proteins,^{9–11} with the dynamic nature of the coordination bonds being utilized to develop responsive films,^{12,13} self-healing soft materials,^{14–16} subcomponent self-assembly of polymeric materials,^{17–21} and hierarchical assemblies of nanoparticles.^{22,23} However, the only example of metal ion coordination leading to a controllable change in the morphology in an aqueous amphiphilic self-assembled system is demonstrated with natural siderophores that are secreted by marine bacteria.^{24,25} Butler and co-workers

have demonstrated that these siderophores, composed of a hydrophilic peptide-based chelator and a fatty acid tail, can undergo an unprecedented metal-induced morphology transition. In the absence of metal ions, assembly occurs to give micelles, while coordination with an excess of Fe(III), Zn(II), Cd(II), or La(III) results in dimerization of the amphiphile, inducing a substantial shift in the packing parameter and formation of new morphologies (vesicles or multilamellar vesicles).

RESULTS AND DISCUSSION

Inspired by these natural siderophore systems, we sought to design a synthetic amphiphile that forms tunable morphologies in the presence of different transition metal ions (Figure 1). A modular synthetic approach was therefore devised based on a tunable macromolecular hydrophobic unit^{26–28} and a peptide chelator (Scheme 1).^{29,30} Oligostyrene was selected as the hydrophobic tail due to its high hydrophobicity, chemical inertness, and glass transition temperature above room temperature. These features impart chemical and kinetic stability to the assembled structures. Hexahistidine, known to dimerize in the presence of transition metal ions,^{9,31,32} was chosen as the hydrophilic chelating domain. Key features of this design are the high degree of structural control over functionality and molecular weight with the peptide component

Received: October 18, 2017

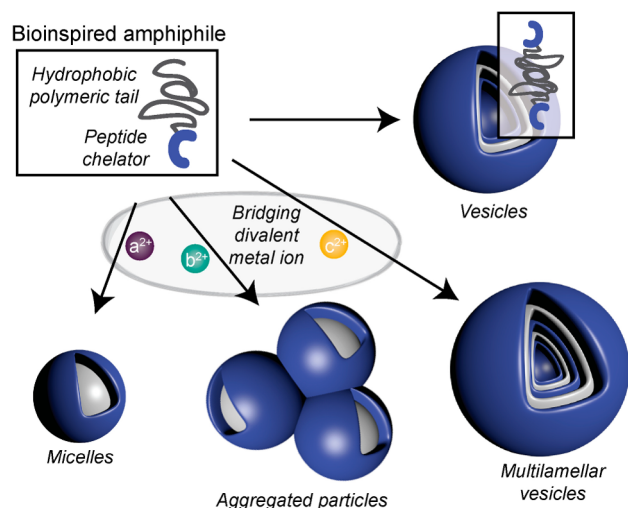
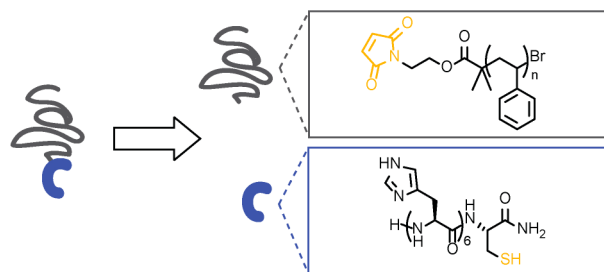


Figure 1. Schematic illustrating a single amphiphilic material that can be transformed into a variety of unique morphologies in response to the presence of different divalent transition metal ions.

Scheme 1. Modular Design Strategy for the Synthesis of $\text{oSt}(\text{His})_6$



being discrete and the synthetic oligomer with a narrow distribution ($D = 1.2$). This allows accurate tuning of assembly and dynamic behavior.

To probe the impact of metal ions on the assembly, a metal-free synthesis of the amphiphile was required. Therefore, efficient and metal-free chemistry (thiol–maleimide reaction) was selected to couple the peptide and oligostyrene.³³ To increase the modularity of this system, polymerization from a preformed, protected maleimide initiator was employed with atom transfer radical polymerization (ATRP),³⁴ allowing for a more controlled polymerization, noncoordinating chain ends, and limited *in situ* deprotection of the initiator (Figure 2a). Oligomers (degree of polymerization (DP) < 10) of styrene were targeted to provide a hydrophobic block of comparable molecular weight to drive the self-assembly of a peptide containing a hexahistidine unit with a terminal cysteine for conjugation to the maleimide. A narrow molecular weight distribution centered at a pentamer and high retention of the furan-protected chain end was confirmed by size exclusion chromatography (SEC) and ¹H NMR analysis (Figure 2b, Figure S3). The reactive maleimide was then exposed by heating the oligostyrene to 120 °C to release the furan followed by coupling to the peptide in DMF with HEPES buffer salt. Quenching with 0.1% trifluoroacetic acid (TFA) then gave the crude peptide–oligomer amphiphile (Figure 3a), which was initially characterized by high-performance liquid chromatography (HPLC). Isolation and purification of amphiphiles is traditionally challenging, and therefore the stoichiometry of the

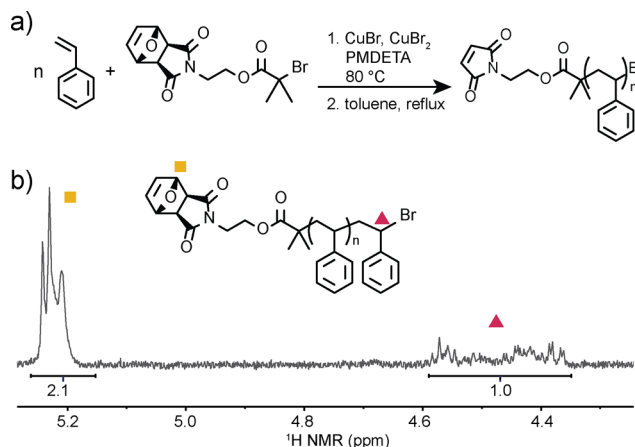


Figure 2. Synthesis of maleimide-terminated oligostyrene. (a) Synthetic scheme; (b) ¹H NMR spectrum of the protected-maleimide oligomer demonstrating chain end fidelity.

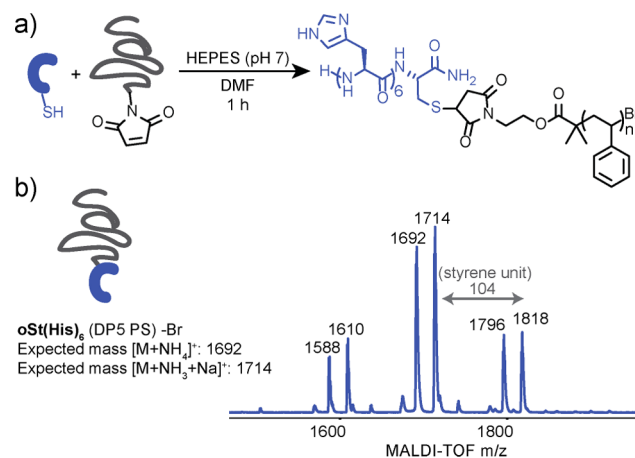


Figure 3. (a) Synthetic scheme for the coupling of oligostyrene to hexahistidine peptide via maleimide–cysteine reaction; (b) MALDI MS confirming synthesis of the peptide–polymer amphiphile. The arrow indicates the difference of a single styrene monomer unit.

coupling reaction was optimized to ensure high yields and minimization of side products. Efficient purification of the desired amphiphile from residual peptide and disulfide dimer was achieved by reverse-phase chromatography eluting with 3:1 water/acetonitrile containing 0.1% TFA to give pure $\text{oSt}(\text{His})_6$, which was fully characterized by mass spectrometry (Figure 3b) and HPLC (Figure S5).

The critical aggregation concentration (CAC) and assembled morphology of $\text{oSt}(\text{His})_6$ were initially studied in the absence of transition metals. The CAC was determined to be less than 10 μM by incubating $\text{oSt}(\text{His})_6$ (concentrations of 0.3–600 μM) with solvatochromic Nile Red using a procedure similar to that described by Stupp and co-workers³⁵ (Figure S6). To ensure complete self-assembly of the amphiphiles, 600 μM was then selected as the concentration of $\text{oSt}(\text{His})_6$ for all subsequent experiments. The assembly proceeded in a noncoordinating buffer,³⁶ HEPES (100 mM, pH 7), at 80 °C for 30 min to allow equilibration above the glass transition temperature of the styrene oligomers. Following imaging with transmission electron microscopy (TEM; cryogenic, Figure 4; negative staining, Figure 5 and Figure S7), vesicle formation was observed in the absence of any divalent metal ions. Additional characterization by dynamic light scattering (DLS,

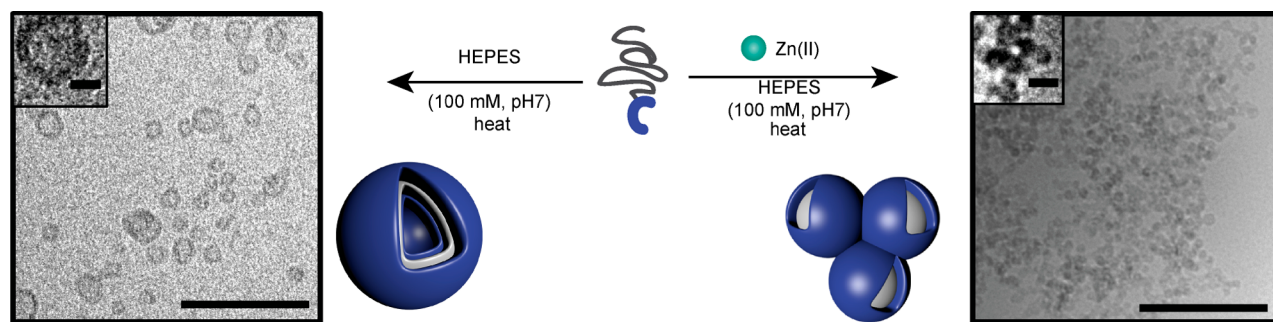


Figure 4. Schematic of the oSt(His)₆ and assembled structures in the absence (left) and presence (right) of Zn(II) (15 mM) in addition to cryo-TEM images. Scale bars represent 200 nm (larger image) and 20 nm (inset image).

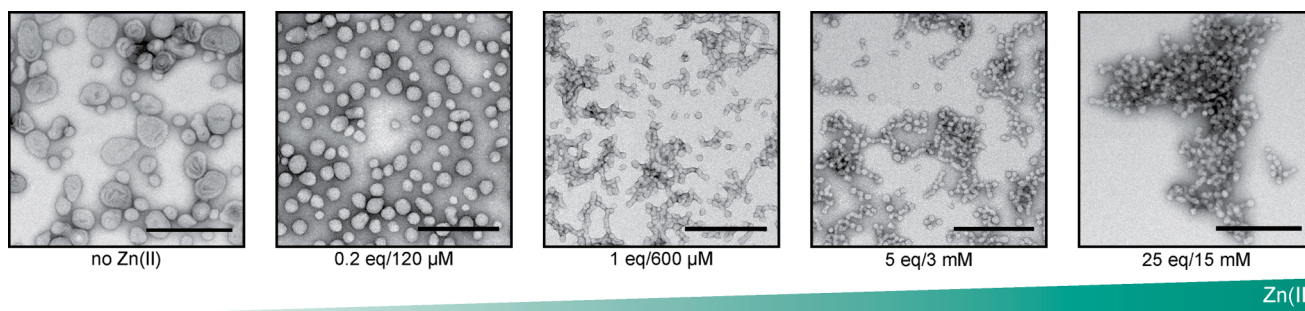


Figure 5. Varying concentrations of Zn(II) lead to different degrees of aggregation. Negative-stained TEM images of oSt(His)₆ (600 μM) assembled with 0–15 mM Zn(II). Negative staining was performed with uranium formate, and all scale bars represent 200 nm. All assembly was performed in buffered solution (HEPES, 100 mM, pH 7).

Figure S15) confirmed vesicle formation with only minimal aggregation. This low level of aggregation is presumably due to secondary interactions between the noncoordinating zwitterionic buffer and the positively charged peptide corona.

Zinc has been previously demonstrated to dimerize hexahistidine peptides³¹ and was initially investigated for directing amphiphile assembly. An excess of Zn(II) (15 mM) was therefore added to a buffered oSt(His)₆ solution (600 μM oSt(His)₆ and 100 mM HEPES) at a neutral pH (confirmed with bromothymol blue) and assembly conducted by heating the mixture to 80 °C and slowly cooling it to room temperature. Imaging with TEM (cryogenic, Figure 4; negative staining, Figure 5 and Figure S7) revealed a definitive change in morphology. In direct contrast to the vesicles formed in the absence of transition metals, zinc induced the formation of networks of aggregated micelles. It is particularly noteworthy that the metal ion was able to both change the size of the spherical assembly and lead to network-like aggregates.

The impact of zinc concentration, temperature, ionic strength, and salt counterion on the assembly was then examined to probe the factors controlling the formation of the aggregated micelle networks. Incubating oSt(His)₆ with increasing concentrations of ZnCl₂ from 120 μM (~0.1 equiv, with respect to oSt(His)₆) to 15 mM (~25 equiv) results in an observable transition from vesicles to micelles to aggregated micelles (Figure 5 and Figure S8). Further characterization was performed at 15 mM Zn(II), as this provides the clearest difference in morphology when compared to the metal-free assemblies. To monitor formation of these networks, samples were heated at 40, 60, and 80 °C, all above the *T_g* of the oligostyrene (34 °C), and the respective morphologies characterized via TEM after different incubation times (Figure S6e). Significantly, the incorporation of micelles

into the aggregated network was observed to increase with increasing temperature (Figure 6, Figure S6). For each 20 °C decrease in temperature, approximately 4 times longer was required for full incorporation into aggregated networks. Samples heated to 40 °C do not appear to assemble fully,

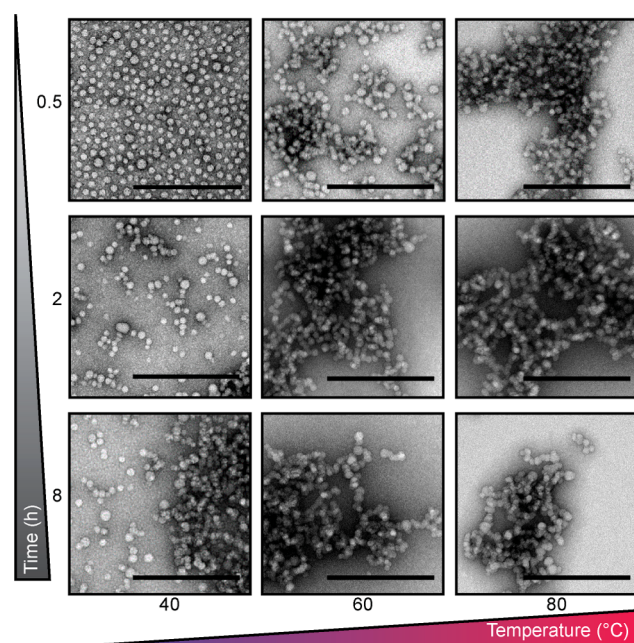


Figure 6. TEM images of oSt(His)₆ assembled in the presence of Zn(II) with different incubation times and temperatures. Samples negatively stained with uranium formate. All scale bars represent 200 nm.

likely due to this temperature being close to the reported T_g . Additionally, networks that were assembled at 80 °C (30 min) were cycled again through the same assembly conditions and demonstrated to be unaffected by reheating (Figure S8a), confirming the robustness of the final morphology. The impact of diluting the structure postassembly was tested via imaging a 10-fold dilution of the original assembled solution (Figure S8b), revealing a similar aggregated network morphology. PIPES, as an alternative to HEPES (Figure S8c), and $Zn(NO_3)_2$ and $Zn(OAc)_2$ (Figure S8e) as replacements for $ZnCl_2$, also led to the assembly of a network of aggregated micelles as visualized by TEM. Finally, when $Zn(II)$ was replaced by noncoordinating $Mg(II)$, spherical assemblies similar to those formed under metal-free conditions were observed (Figure S8d), reinforcing that specific interactions between the peptide domain of the amphiphile and $Zn(II)$ lead to the network morphology.

Encouraged by the morphological change induced by $Zn(II)$, additional transition metal ions were selected to evaluate how ions with different properties (e.g., ionic radius and coordination stoichiometry/geometry) impact assembly. Under identical conditions, assembly of $oSt(His)_6$ in the presence of $Mn(II)$, $Co(II)$, $Ni(II)$, $Cu(II)$, $Cd(II)$, and $Fe(III)$ was conducted, leading to a diverse array of morphologies (Figure 7, Figure S14, DLS Figure S15, negatively stained TEM Figures S9–13). $Co(II)$ -directed assembly led to aggregated micelle networks similar to those formed in the presence of $Zn(II)$, as visualized by cryogenic TEM. Comparable aggregation was also observed in the presence of $Cu(II)$ with preliminary cryo-TEM visualization showing a more organized network. In contrast, $Mn(II)$ -, $Ni(II)$ -, and $Cd(II)$ -directed assembly led to isolated particles as characterized by TEM and DLS, indicating that these metal ions did not induce secondary aggregation (Figure 7). Interestingly, micelles were observed in the presence of $Ni(II)$ and $Cd(II)$, whereas multilamellar vesicles were formed in the presence of $Mn(II)$. A hollow core and thick corona with faint rings can be observed in the cryogenic images. Assembly in PIPES buffer allowed for clear visualization of multiple layers (Figure S13d); the particles formed in this buffer are larger, likely due to the higher ionic strength, as has been observed with phospholipids.³⁷ On progressing to the $Fe(III)$ ion, only unstructured aggregates that separated from the aqueous solution were observed (Figure S14). The wide range of morphologies obtained clearly indicate that the nature of the transition metal ion and associated atomic-scale differences in coordination significantly affects nanoscale assembly, further highlighting the promise of metal binding in the development of responsive materials.

Intrigued by the observation that $Ni(II)$ and $Cd(II)$, ions with relatively large differences in ionic radius, both assembled into micelles, we turned our attention to the role of coordination geometry. With the exception of $Mn(II)$, all of the ions have been demonstrated to dimerize hexahistidine;³¹ therefore, we hypothesized that the structures are composed of amphiphiles binding in a 2:1 $oSt(His)_6$:metal ion ratio. Different binding geometries of these 2:1 coordination complexes may lead to the distinct assemblies visualized by cryo-TEM. For proteins engineered to contain imidazole-based binding sites, X-ray crystallography³⁸ has shown a tetrahedral binding geometry for $Zn(II)$,³⁹ square planar for $Cu(II)$, and octahedral for $Ni(II)$.⁴⁰ On the basis of these reported assembly profiles,⁴¹ we propose coordination modes for each of the morphologies (Figure 7) with square-planar ($Cu(II)$) and

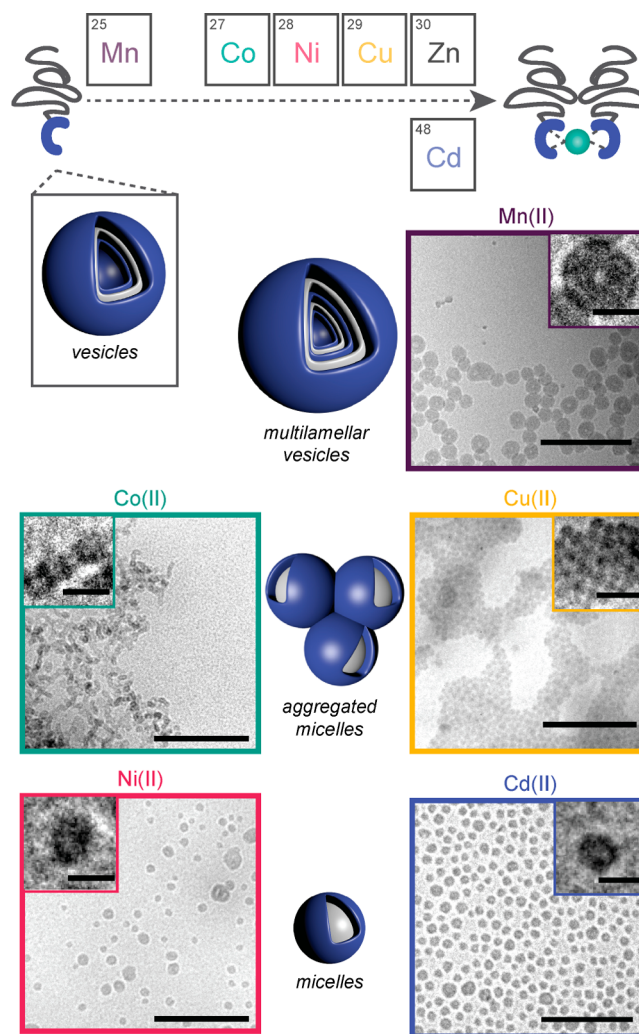


Figure 7. Assembly of $oSt(His)_6$ in the presence of divalent transition metals. Cryo-TEM images show $oSt(His)_6$ assembled in the presence of $Mn(II)$, multilamellar vesicles; $Co(II)/Cu(II)$, aggregated micelles; and $Ni(II)/Cd(II)$, micelles. Scale bars represent 200 nm (larger image) and 20 nm (inset image).

tetrahedral ($Zn(II)$ and $Co(II)$) leading to aggregated micelle networks, whereas an octahedral geometry ($Ni(II)$ and $Cd(II)$) with coordinated water (common in proteins⁴¹ and observed in subcomponent assembly²⁰) leads to isolated micelles. Unlike the prior transition metal ions, $Mn(II)$ does not dimerize hexahistidine¹ and assembly is dictated by binding stoichiometry instead of geometry. To further evaluate this difference, $oSt(His)_6$ was assembled in the presence of differing stoichiometries of $Mn(II)$ and $Ni(II)$ with the size of the resulting nanostructures being characterized by DLS. As shown in Figure 8, only 0.5 equiv of $Ni(II)$ are needed for micelle formation, while approximately 5.0 equiv are required for $Mn(II)$ to form the final multilamellar vesicle. We therefore conclude that multiple $Mn(II)$ ions are bound to each $oSt(His)_6$.

CONCLUSIONS

In conclusion, we describe the formation of tunable nanoscale morphologies directed by metal ion coordination. A peptide polymer amphiphile, $oSt(His)_6$, was synthesized with a modular strategy and observed to assemble into vesicles in the absence

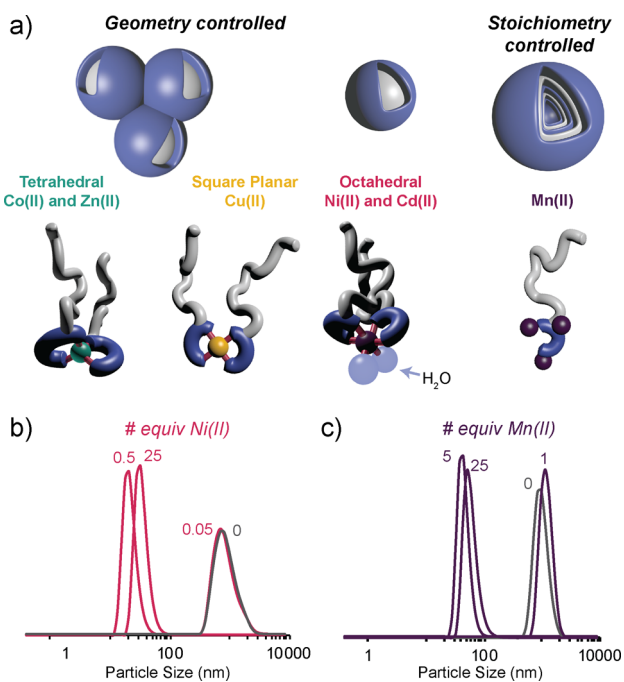


Figure 8. Proposed binding modes of oSt(His)₆ to divalent transition metals. (a) Illustration of the proposed coordination of oSt(His)₆ to divalent ions. Number distributions from DLS for oSt(His)₆ assembled in the presence of different numbers of equivalents of (b) Ni(II) and (c) Mn(II).

of transition metals and aggregated particles in the presence of Zn(II). The aggregation was determined to be due to the coordination of the Zn(II) ion. Aggregated particles were also observed in the presence of Co(II) and Cu(II), isolated micelles directed by Ni(II) and Cd(II) were observed, and multilamellar vesicles were formed when oSt(His)₆ coordinated to Mn(II). Proposed models for binding geometry and stoichiometry illustrate the control over nanoscale morphologies dictated by small differences in the nature of the transition metal ion. This design principle illustrates the wide variety of nanoscale materials that can be assembled from a well-defined oligomer–peptide amphiphile and provides an attractive avenue for the development of multistimuli-responsive nanomaterials. Future directions of this work are aimed at continuing to probe the mechanism and limitations of the role of metal ions in directing the assembly of amphiphiles.

■ ASSOCIATED CONTENT

Supporting Information

The Supporting Information is available free of charge on the ACS Publications website at DOI: 10.1021/jacs.7b11005.

Full experimental procedures and additional characterization data (PDF)

■ AUTHOR INFORMATION

Corresponding Authors

*aknight@berkeley.edu

*hawker@mrl.ucsb.edu

ORCID

Craig J. Hawker: 0000-0001-9951-851X

Notes

The authors declare no competing financial interest.

■ ACKNOWLEDGMENTS

This work was supported primarily by the National Science Foundation (MRSEC program DMR 1720256). Work at the Molecular Foundry was supported by the Office of Science, Office of Basic Energy Sciences, of the U.S. Department of Energy under Contract No. DE-AC02-05CH11231. A.S.K. was supported by a postdoctoral fellowship from the Arnold and Mabel Beckman Foundation. J.M.R. thanks the Victorian Endowment for Science, Knowledge and Innovation (VESKI) for a postdoctoral fellowship.

■ REFERENCES

- (1) Coleman, A. C.; Beierle, J. M.; Stuart, M. C.; Maciá, B.; Caroli, G.; Mika, J. T.; van Dijken, D. J.; Chen, J.; Browne, W. R.; Feringa, B. L. *Nat. Nanotechnol.* **2011**, *6*, 547–552.
- (2) Jang, S. G.; Audus, D. J.; Klinger, D.; Krogstad, D. V.; Kim, B. J.; Cameron, A.; Kim, S.-W.; Delaney, K. T.; Hur, S.-M.; Killups, K. L.; Fredrickson, G. H.; Kramer, E. J.; Hawker, C. J. *J. Am. Chem. Soc.* **2013**, *135*, 6649–6657.
- (3) Moughton, A. O.; O'Reilly, R. K. *Chem. Commun.* **2010**, *46* (7), 1091–1093.
- (4) Yan, Q.; Zhao, Y. *Angew. Chem., Int. Ed.* **2013**, *52*, 9948–9951.
- (5) Sato, S.; Murase, T.; Fujita, M. *Supramolecular Chemistry: From Molecules to Nanomaterials*; John Wiley & Sons, Ltd: Hoboken, 2012.
- (6) Geng, Y.; Wang, X.-J.; Chen, B.; Xue, H.; Zhao, Y.-P.; Lee, S.; Tung, C.-H.; Wu, L.-Z. *Chem. - Eur. J.* **2009**, *15*, 5124–5129.
- (7) Li, L.; Ke, C.-F.; Zhang, H.-Y.; Liu, Y. *J. Org. Chem.* **2010**, *75*, 6673–6676.
- (8) Xiao, Z.-Y.; Zhao, X.; Jiang, X.-K.; Li, Z.-T. *Chem. Mater.* **2011**, *23*, 1505–1511.
- (9) Van Eldijk, M. B.; Schoonen, L.; Cornelissen, J. J. L. M.; Nolte, R. J. M.; Van Hest, J. C. M. *Small* **2016**, *12*, 2476–2483.
- (10) Salgado, E. N.; Radford, R. J.; Tezcan, F. A. *Acc. Chem. Res.* **2010**, *43*, 661–672.
- (11) Nepal, M.; Sheedlo, M. J.; Das, C.; Chmielewski, J. *J. Am. Chem. Soc.* **2016**, *138*, 11051–11057.
- (12) Kumpfer, J. R.; Rowan, S. J. *ACS Macro Lett.* **2012**, *1*, 882–887.
- (13) Michal, B. T.; McKenzie, B. M.; Felder, S. E.; Rowan, S. J. *Macromolecules* **2015**, *48*, 3239–3246.
- (14) Mozhdehi, D.; Ayala, S.; Cromwell, O. R.; Guan, Z. *J. Am. Chem. Soc.* **2014**, *136*, 16128–16131.
- (15) Grindy, S. C.; Learsch, R.; Mozhdehi, D.; Cheng, J.; Barrett, D. G.; Guan, Z.; Messersmith, P. B.; Holten-Andersen, N. *Nat. Mater.* **2015**, *14*, 1181–1292.
- (16) Whittell, G. R.; Hager, M. D.; Schubert, U. S.; Manners, I. *Nat. Mater.* **2011**, *10*, 176–188.
- (17) Ott, C.; Hoogenboom, R.; Hoepfner, S.; Wouters, D.; Gohy, J.-F.; Schubert, U. S. *Soft Matter* **2008**, *5*, 84–91.
- (18) Gao, H.; Liu, G.; Chen, X.; Hao, Z.; Tong, J.; Lu, L.; Cai, Y.; Long, F.; Zhu, M. *Macromolecules* **2010**, *43*, 6156–6165.
- (19) Chen, X.; Xu, N.; Li, N.; Lu, L.; Cai, Y.; Zhao, Y.; Wang, D. *Soft Matter* **2013**, *9*, 1885–894.
- (20) Wu, X.; Xu, N.; Zhu, Z.; Cai, Y.; Zhao, Y.; Wang, D. *Polym. Chem.* **2014**, *5*, 1202–1209.
- (21) Xu, N.; Han, J.; Zhu, Z.; Song, B.; Lu, X.; Cai, Y. *Soft Matter* **2015**, *11*, 5546–5553.
- (22) Wang, Y.; Hollingsworth, A. D.; Yang, S. K.; Patel, S.; Pine, D. J.; Weck, M. *J. Am. Chem. Soc.* **2013**, *135*, 14064–14067.
- (23) Lunn, D. J.; Gould, O. E. C.; Whittell, G. R.; Armstrong, D. P.; Mineart, K. P.; Winnik, M. A.; Spontak, R. J.; Pringle, P. G.; Manners, I. *Nat. Commun.* **2016**, *7*, 12371.
- (24) Martinez, J. S.; Zhang, G. P.; Holt, P. D.; Jung, H.-T.; Carrano, C. J.; Haygood, M. G.; Butler, A. *Science* **2000**, *287*, 1245–1247.
- (25) Butler, A.; Theisen, R. M. *Coord. Chem. Rev.* **2010**, *254*, 288–296.
- (26) Chen, C.; Wylie, R. A. L.; Klinger, D.; Connal, L. A. *Chem. Mater.* **2017**, *29*, 1918–1945.

- (27) Roy, D.; Cambre, J. N.; Sumerlin, B. S. *Prog. Polym. Sci.* **2010**, *35*, 278–301.
- (28) Stuart, M. A. C.; Huck, W. T. S.; Genzer, J.; Müller, M.; Ober, C.; Stamm, M.; Sukhorukov, G. B.; Szleifer, I.; Tsukruk, V. V.; Urban, M.; Winnik, F.; Zauscher, S.; Luzinov, I.; Minko, S. *Nat. Mater.* **2010**, *9*, 101–113.
- (29) Cui, H.; Webber, M. J.; Stupp, S. I. *Biopolymers* **2010**, *94*, 1–18.
- (30) Mikhalevich, V.; Craciun, I.; Kyropoulou, M.; Palivan, C. G.; Meier, W. *Biomacromolecules* **2017**, *18*, 3471–3480.
- (31) Evers, T. H.; Appelhof, M. A. M.; Meijer, E. W.; Merckx, M. *Protein Eng., Des. Sel.* **2008**, *21*, 529–536.
- (32) Valenti, L. E.; De Pauli, C. P.; Giacomelli, C. E. *J. Inorg. Biochem.* **2006**, *100* (2), 192–200.
- (33) Velonia, K.; Rowan, A. E.; Nolte, R. J. M. *J. Am. Chem. Soc.* **2002**, *124*, 4224–4225.
- (34) Mantovani, G.; Lecolley, F.; Tao, L.; Haddleton, D. M.; Clerx, J.; Cornelissen, J. J. L. M.; Velonia, K. *J. Am. Chem. Soc.* **2005**, *127*, 2966–2973.
- (35) Moyer, T. J.; Finbloom, J. A.; Chen, F.; Toft, D. J.; Cryns, V. L.; Stupp, S. I. *J. Am. Chem. Soc.* **2014**, *136*, 14746–14752.
- (36) Good, N. E.; Winget, G. D.; Winter, W.; Connolly, T. N.; Izawa, S.; Singh, R. M. M. *Biochemistry* **1966**, *5*, 467–477.
- (37) Kodama, M.; Miyata, T. *Thermochim. Acta* **1995**, *267*, 365–372.
- (38) Bailey, J. B.; Subramanian, R. H.; Churchfield, L. A.; Tezcan, F. A. *Methods Enzymol.* **2016**, *580*, 223–250.
- (39) Salgado, E. N.; Faraone-Mennella, J.; Tezcan, F. A. *J. Am. Chem. Soc.* **2007**, *129*, 13374–13375.
- (40) Salgado, E. N.; Lewis, R. A.; Mossin, S.; Rheingold, A. L.; Tezcan, F. A. *Inorg. Chem.* **2009**, *48*, 2726–2728.
- (41) Harding, M. M.; Nowicki, M. W.; Walkinshaw, M. D. *Crystallogr. Rev.* **2010**, *16*, 247–302.